5101-211
Flat-Plate
Solar Array Project

DOE/JPL-1012-73
Distribution Category UC-63b

Experimental Evaluation of the Battelle Accelerated Test Design

For the Solar Array at Mead, Nebraska

P.O. Frickland
J. Repar

April 6, 1982

Prepared for
U.S. Department of Energy
Through an Agreement with
National Aeronautics and Space Administration
by
Jet Propulsion Laboratory
California Institute of Technology
Pasadena, California

(JPL PUBLICATION 82-52)

5101-211
Flat-Plate
Solar Array Project

DOE/JPL-1012-73
Distribution Category UC-63b

Experimental Evaluation of the Battelle Accelerated Test Design

For the Solar Array at Mead, Nebraska

P.O. Frickland
J. Repar

April 6, 1982

Prepared for
U.S. Department of Energy
Through an Agreement with
National Aeronautics and Space Administration
by
Jet Propulsion Laboratory
California Institute of Technology
Pasadena, California

(JPL PUBLICATION 82-52)

Prepared by the Jet Propulsion Laboratory, California Institute of Technology, for the U.S. Department of Energy through an agreement with the National Aeronautics and Space Administration.

The JPL Flat-Plate Solar Array Project is sponsored by the U.S. Department of Energy and is part of the Photovoltaic Energy Systems Program to initiate a major effort toward the development of cost-competitive solar arrays.

This publication reports on work done under NASA Task RD-152, Amendment 66, DOE/NASA IAA No. DE-AI01-76ET20356.

ABSTRACT

A previously developed test design for accelerated aging of photovoltaic modules was experimentally evaluated. The studies included a review of relevant field experience, environmental chamber cycling of full-size modules, and electrical and physical evaluation of the effects of accelerated aging during and after the tests. The test results indicated that thermally induced fatigue of the interconnects was the primary mode of module failure as measured by normalized power output. No chemical change in the silicone encapsulant was detectable after 360 test cycles.

ACKNOWLEDGMENTS

This study was made possible by the close support of several people at the Jet Propulsion Laboratory (JPL). Implementation of the environmental testing was accomplished with the assistance of Cliff Nelson. Module performance evaluation employed the JPL Flat-Plate Solar Array Project's Large-Area Pulsed Solar Simulator Facility, where testing was coordinated through John Griffith. Physical and chemical evaluation of the aged modules was performed by Robert Gauldin and Lois Taylor. Background studies in the area of interconnect fatigue failure modeling were provided by Don Moore and Gordon Mon. Mathematical analysis was supported by Jerry Millard and James Jeffery.

Special appreciation is expressed to Steve Foreman of Massachusetts Institute of Technology (MIT) for providing background information on MIT's field-testing program.

GLOSSARY

ABBREVIATIONS AND ACRONYMS

DOE	U.S. Department of Energy
FSA	Flat-Plate Solar Array Project
IC	interconnect(s)
I/V	current/voltage
JPL	Jet Propulsion Laboratory
LAPSS	large-area pulsed solar simulator
MIT-LL	Massachusetts Institute of Technology - Lincoln Laboratory
NOCT	nominal operating cell temperature
P/N	part number
PV	photovoltaic(s)
RH	relative humidity
RTV	room-temperature vulcanized (rubber)
S/N	serial number
UV	ultraviolet

CONTENTS

Tables

SECTION I

INTRODUCTION

One of the purposes of the Environmental Isolation Task of the Flat-Plate Solar Array (FSA) Project at the Jet Propulsion Laboratory (JPL) is to develop accelerated test methodologies for photovoltaic (PV) arrays and constituent materials. Under this task, an accelerated test design for use in predicting the life expectancy of the 25-kW array located at Mead, Nebraska, was developed and evaluated. This was a two-part effort that was accomplished jointly by Battelle Columbus Laboratories (test design development) and JPL (experimental validation studies).

The test-design development included studies in the following three areas:

(1) The development of an appropriate test-design methodology, which included the number of tests to be performed, the expected aging modes, and the distribution of test samples among the various test conditions (Reference 1).

(2) A review and limited experimental assessment of measurement techniques, which could be useful in determining degradation of the many elements and interfaces of the module, (References 2 and 3).

(3) The test design itself (Reference 4).

The experimental evaluation of the test design is the subject of this report. The experimental studies included:

(1) Exposure of PV modules to a cyclic-temperature, high-humidity, and constant-pollutant environment.

(2) Periodic visual and electrical evaluation.

(3) Microscopic and chemical analysis of artificially aged modules.

(4) Comparison of artificially aged modules and modes of failure with the Mead array and unaged reference modules.

SECTION II

ACCELERATED TEST DESIGN

A. BACKGROUND

The objective of the accelerated test design was to furnish a method for predicting 20+ years of solar-array service life with less than 2 years of actual testing. Based on an assessment of available module and material performance data, Battelle predicted the following factors as being the most probable contributers to performance degradation:

(1) Increase in cell series resistance (R_S).

(2) Delamination of cover.

(3) Interconnect breakage.

(4) Cell cracking.

(5) Increase in bulk absorptivity of the materials in the optical path to the cell.

(6) Interconnect corrosion.

These factors (or modes) were expected to be a consequence of the specific interactive and noninteractive stresses to which the modules would be exposed.

Potentially interactive stresses that were identified were insolation [ultraviolet (UV) components], temperature, temperature cycling, moisture, mechanical forces, and chemical contamination. Strong interaction was predicted for the moisture-chemical contamination, temperature-moisture, and temperature-mechanical combinations. Surface soiling, hail, cell back-bias, and thermal shock were tentatively identified as noninteractive stresses that could be treated independently, allowing simplification of the experimental design.

B. GENERAL TEST-DESIGN FORMULATION

The test design was restricted to long-term degradation as measured by change in power output. More specifically, the dependent variable was taken to be $P_{(t)}/P_{(o)}$, where $P_{(t)}$ is the power output at time, t, under standard conditions of insolation and temperature; and $P_{(o)}$ is the initial power output ($t = 0$). Test completion was defined as the point where average $P_{(t)}/P_{(o)} = 0.5$. The basic correlation that was employed was

$$\frac{P_{(t)}}{P_{(o)}} = (1 - kt)^{1/\beta} \qquad (1)$$

The effect of various values for the shape factor, β, is shown in Figure 2-1. The rate constant, k, is a function of the various applied nonthermal stresses. The specific relationship assumed was

$$k = A e^{-B/T} (1 + f_1)^{a_1} (1 + f_2)^{a_2} \cdots (1 + f_i)^{a_i} \quad (2)$$

where f_i represents a specific stress [e.g., relative humidity (RH)], A and B are constants, and T is temperature. The exponent a_i was also expressed as a function of temperature:

$$a_i = C_1 - \frac{C_2}{T} \quad (3)$$

where C_1 and C_2 are constants.

Based upon these relationships, the test design called for evaluating the electrical response of full-size modules and the physical response of material samples in accelerated constant-temperature, cyclic-temperature, and UV environments. By evaluating the response (degradation) at various acceleration (stress) levels, the fundamental dependence of k upon stress level could be determined. This would allow extrapolation to the zero acceleration (Mead solar array) level. Figure 2-2 shows this extrapolation (based on estimates for the various rate parameters) as reported by Battelle.

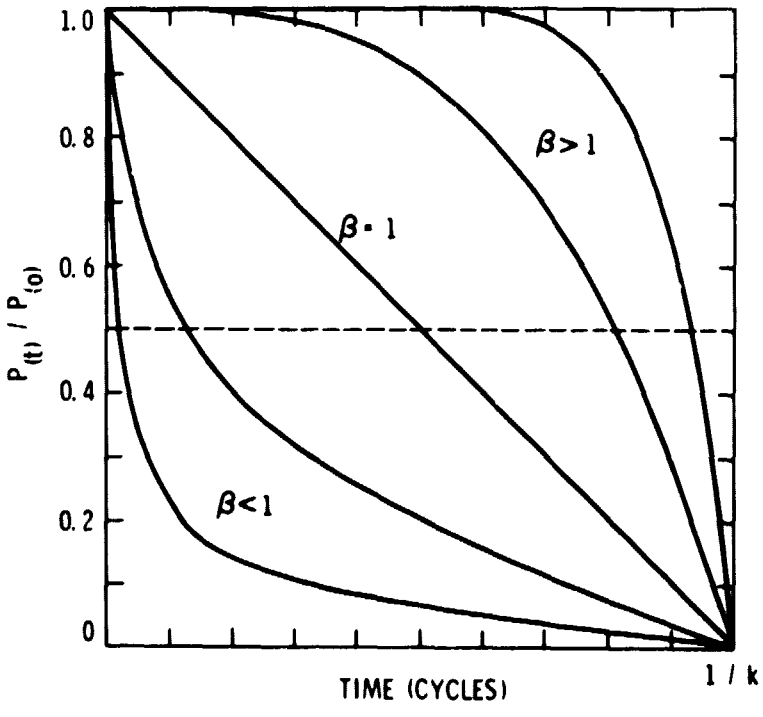

Figure 2-1. Battelle Performance Model

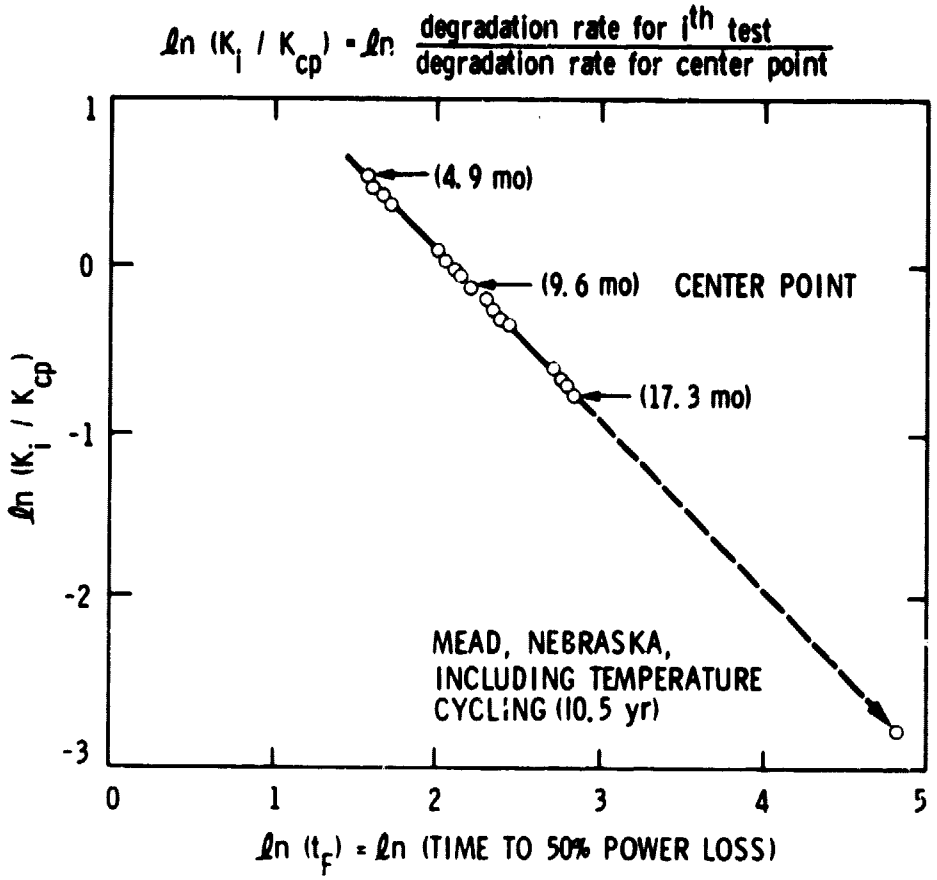

Figure 2-2. Test-Design Points, Degradation Rates, and Anticipated Times to 50% Power Loss for Cyclic-Temperature Tests (Reference 4)

SECTION III

TEST PARAMETER SELECTION

Because of a large number of variables in each part of the test (see Table 3-1), several hundred modules would have been required to fully evaluate the test plan as presented. A full-spectrum evaluation of the test design was not practical, because of the module cost, facilities requirements, and test duration. In the interest of time and cost, a decision was made to evaluate ten modules at the cyclic-temperature test point that has the highest acceleration factor: 1.0 ppm SO_2 concentration, 85% RH, and the temperature cycle shown in Figure 3-1.

Table 3-1. Proposed Variables of Each Part of the Complete Test Design

Test	Variables
Constant Temperature[a]	Temperature, RH, SO_2 concentration
Cyclic Temperature[a]	Temperature, temperature excursion, RH, SO_2 concentration
UV	UV (0.3 to 0.4 μm), temperature, RH

[a]A constant forward-bias current on the modules is included in these tests, along with the application of a static electric field between the output terminal and module frame.

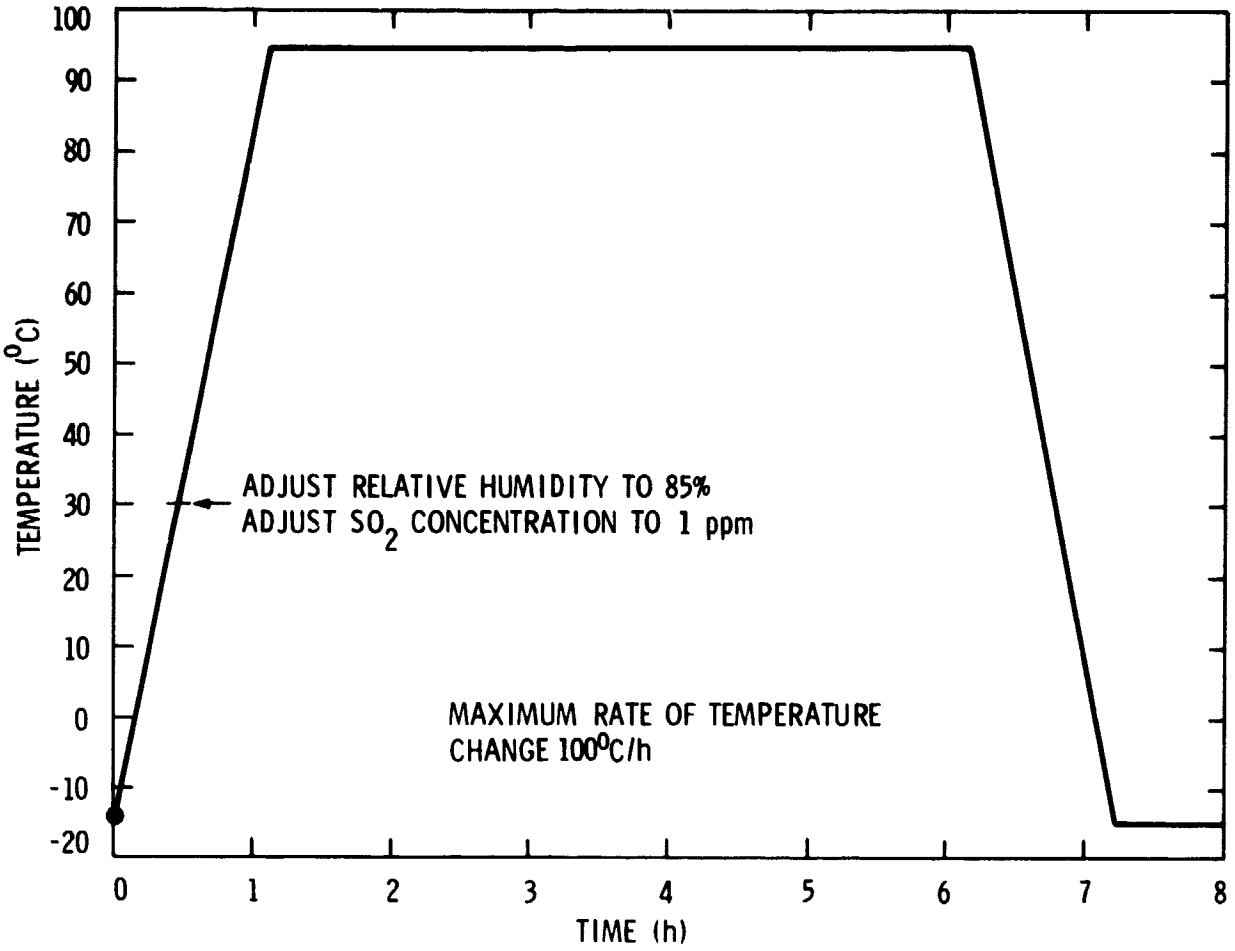

Figure 3-1. Accelerated Test Validation Cycle

SECTION IV

FACILITIES DEVELOPMENT

The specific test-design requirements of this study required the modification of available facilities. Facilities development included the modification of an environmental test chamber to accommodate multistress weathering and adaption of a large-area pulsed solar simulator (LAPSS) facility for performance evaluation of the weathered modules.

A. ENVIRONMENTAL CHAMBER

The requirements for the environmental chamber included provisions for regulating temperature, RH, and SO_2 concentrations as a function of time.

A Bemco temperature chamber (Figure 4-1), Model No. FW100/350-27 with a 3 x 3 x 3 ft interior, was equipped with cam controller/recorders for temperature and humidity. The temperature was continuously controlled whereas humidity was stabilized once each day at 30°C.

The SO_2 modifications included installing gas-inlet controls and a concentration monitor as shown in Figure 4-2. As the SO_2 concentration was adjusted in discreet amounts at a stabilization plateau, an automatic controller was unnecessary. The chamber was, however, found to have numerous small air leaks, requiring the inside of the chamber to be sealed with Mylar film. To accommodate the expansion of the chamber gasses at temperatures above 30°C, a polyethylene reservoir bag was added to the top of the chamber.

Handling, transporting, and positioning of the modules within the environmental chamber were expected to provide some unique problems. These problems were minimized by building a removable stainless-steel rack for the chamber (Figure 4-3). Figure 4-4 illustrates the rack in position in the sealed chamber.

B. LARGE-AREA PULSED SOLAR SIMULATOR

The LAPSS at JPL was used for determining the module electrical performance. The LAPSS (Figure 4-5) consisted of a Xenon lamp source located in a 13-m-long nonreflective chamber. The modules were placed in the chamber with a reference cell and were irradiated with approximately 100 mW/cm^2 for a duration of 3 ms. During the irradiation the modules were subjected to various electrical loads and the response of each module was monitored. This data was then normalized and automatically plotted as the current/voltage (I/V) curves, used to evaluate the condition of the modules. For a detailed discussion of the operation of the LAPSS facility at JPL, refer to Reference 5.

Figure 4-1. Environmental Test Chamber

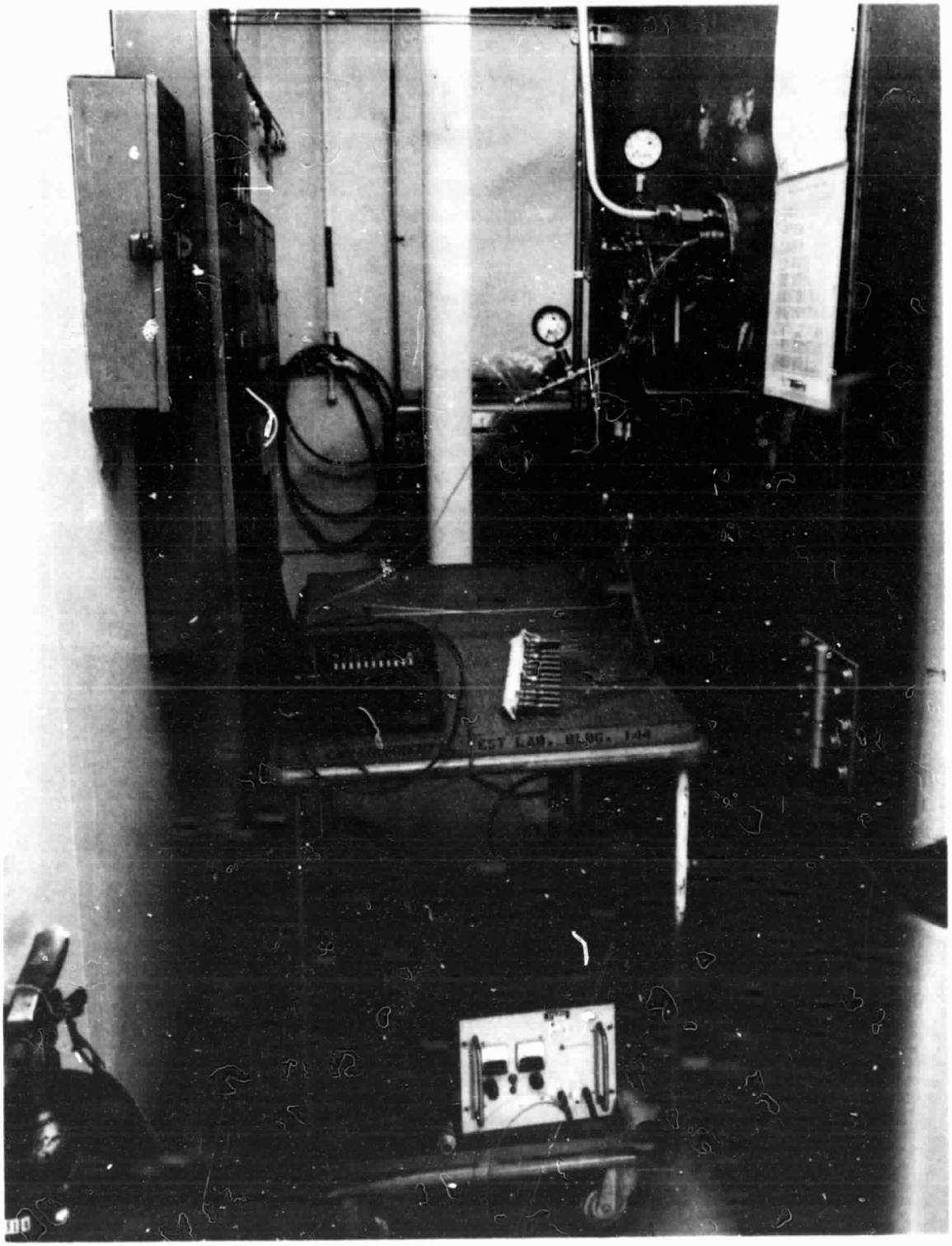

Figure 4-2. Chamber Modifications for SO_2

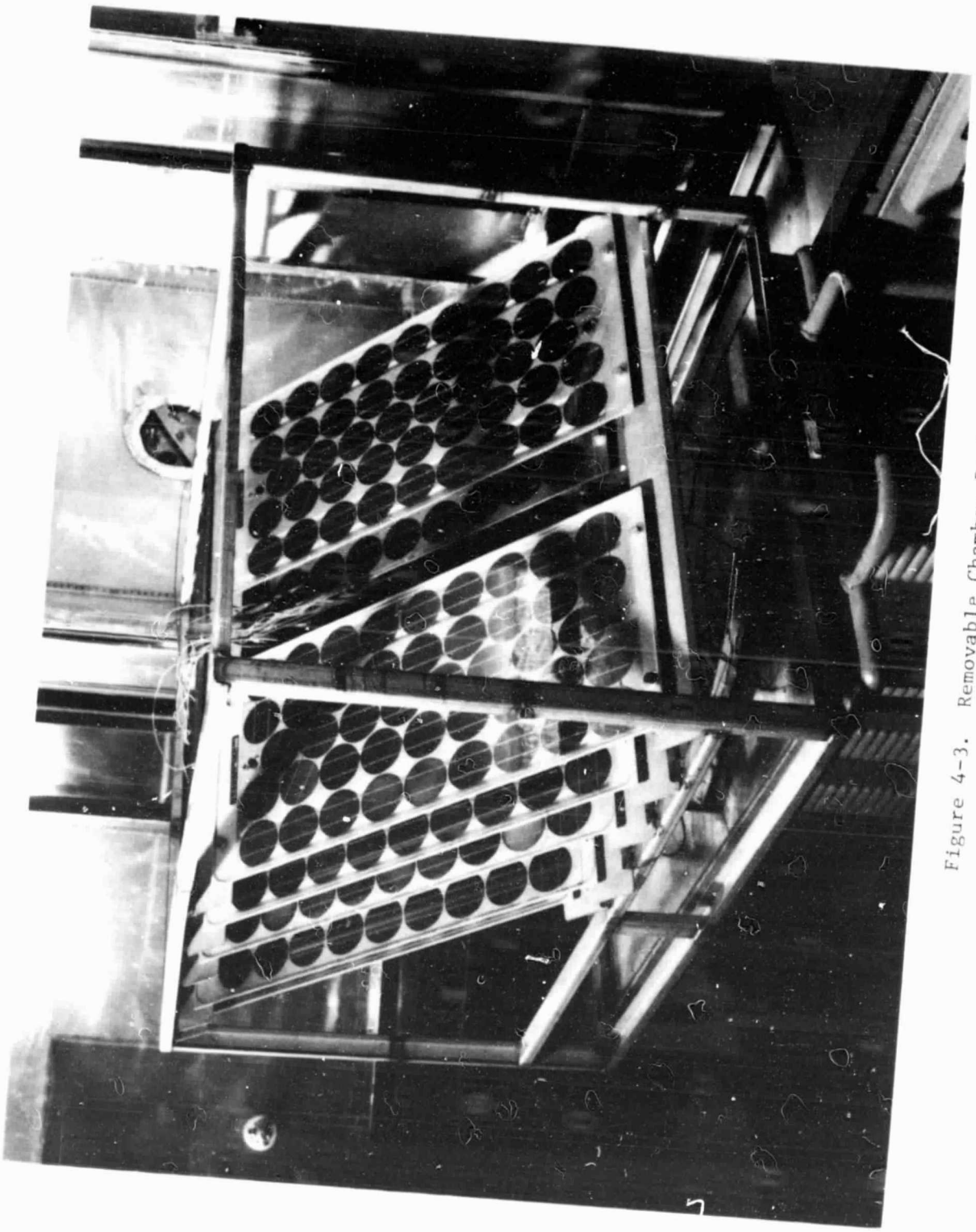

Figure 4-3. Removable Chamber Rack

Figure 4-4. Sealed Chamber

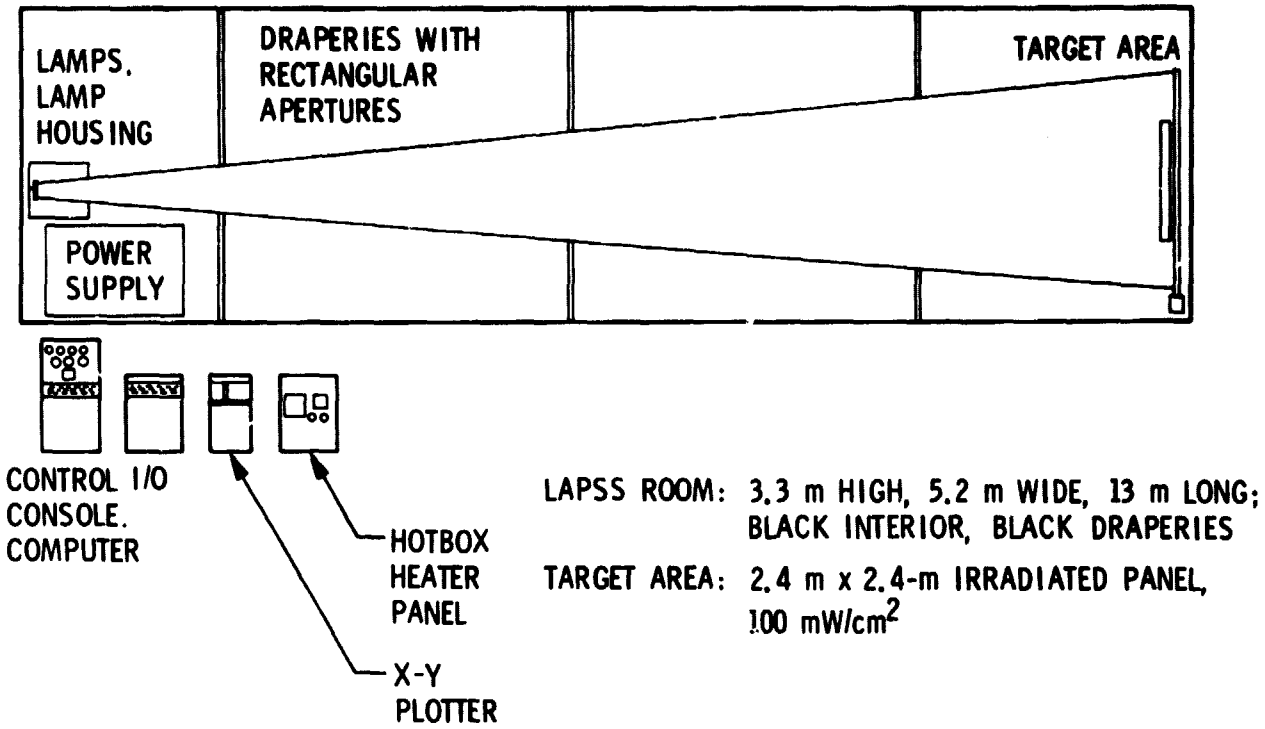

Figure 4-5. Large-Area Pulsed Solar Simulator Facility

SECTION V

REVIEW OF PREVIOUS PERFORMANCE

A. MEAD, NEBRASKA, FIELD-TEST SITE

In July 1977, the Lincoln Laboratory of the Massachusetts Institute of Technology (MIT-LL) activated a 25-kW_p PV power-generating system at the Mead Field Station of the University of Nebraska. The array field consisted of 2240 modules of which 1512 were of the Sensor Technology Block II design. Field inspections of the installation were conducted twice a year for 2-1/2 years. A synopsis of the 1978-79 inspections (Reference 6) is presented as follows.

The physical discrepancies noted in the 1977-79 MIT reports are shown in Table 5-1. These defects represent the types of real-time changes that are typical of silicone rubber-encapsulated modules.

The most prevalent degradation observed after field exposure was encapsulant delamination over the cells, over and around the interconnects, and around the edge seals. Split encapsulant, notably over the cells and interconnects, was also observed.

Table 5-1. Module Physical Degradation at the Mead Field-Test Site

Defects	Modules
Modules inspected	2080
Edge-seal delamination	1037
Newly cracked cells	1044
Delamination over cells	386
Delamination over or around interconnects (IC)	65
Split encapsulation over IC or cell	54
Protruding IC or cell	35
Broken IC detected	0

Notes: (1) Cumulative field-inspection results (all Sensor Technology designs).
(2) Time period of July 1977 to October 1979 (27 months).

The second most prevalent degradation was cell cracking. More than one-half of the modules inspected suffered at least one cracked cell. Most of these were due to hail impact (mainly from a single storm in May 1978), and the rest were due to natural weathering. The cell cracking that was observed is shown in Table 5-2.

At least one cracked cell was observed in 61% of the Sensor Technology modules. Of these cracked cells, 47% were due to impact damage (see Figure 5-1). The remaining 53% were caused apparently by differential thermal expansion of the silicone rubber-filled ribs, which resulted in uneven pressure on the backside of the cells. After 27 months of operation, 2.2% of all cells (of both designs) were cracked.

At Mead, the modules were considered to have failed electrically when the short-circuit current dropped below 75% of nominal for the prevailing conditions. The result of 12 searches for module failures is presented graphically in Figure 5-2.

After 39 months of operation, 4% of the 2240 modules had failed. The rate of module failures was observed to increase after the hailstorm in May 1978. This would indicate that the cells that were cracked by impact constituted incipient failures which required time to develop to the point where they were detectable, using the 75% performance/failure criteria.

Early in 1980, four failures were found among the other types (non Sensor Technology Block II) of modules in the array that could be attributed to interconnect fatigue resulting from differential thermal expansion of the substrate, cells, and interconnects. However, no fatigue failures have been noted to date in the Sensor Technology design.

B. OTHER FIELD-TEST SITES

In another field test, the MIT-LL installed a 15-kW_p PV array at a radio station in Bryon, Ohio. This array consisted of a myriad of module designs.

Table 5-2. Cracked-Cell Data at the Mead Field-Test Site

Manufacturer	Modules Inspected	Modules With Cracked Cells	Total No. of Cracked Cells	No. of Impact Cracked Cells	Total No. of Cells
Total	2080	1044	2021	1155	90,168
Sensor Technology Block II	1404	856	1596	758	61,776

Note: Time period of July 1977 to October 1979 (27 months).

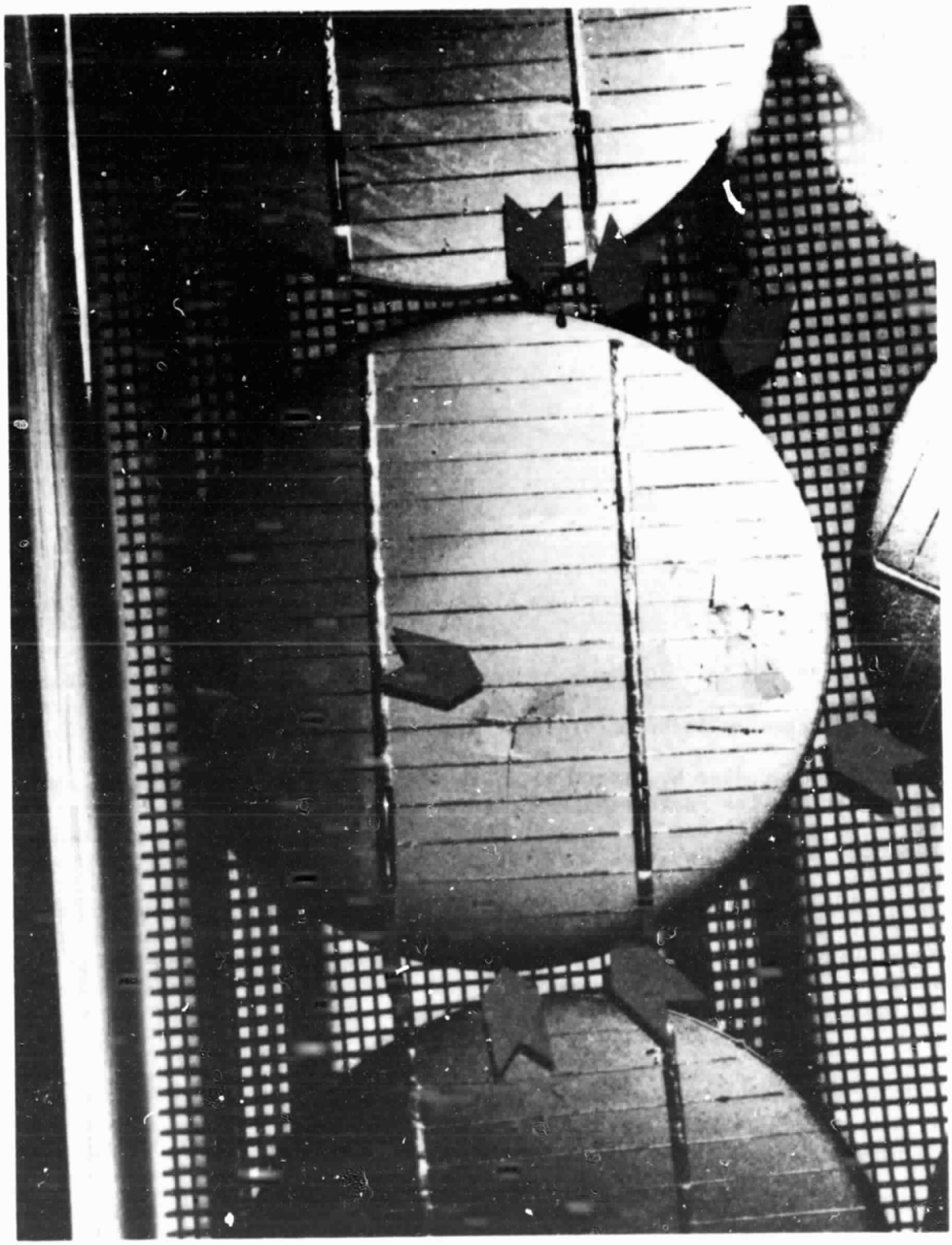

Figure 5-1. Impact Damage at the Mead Field-Test Site

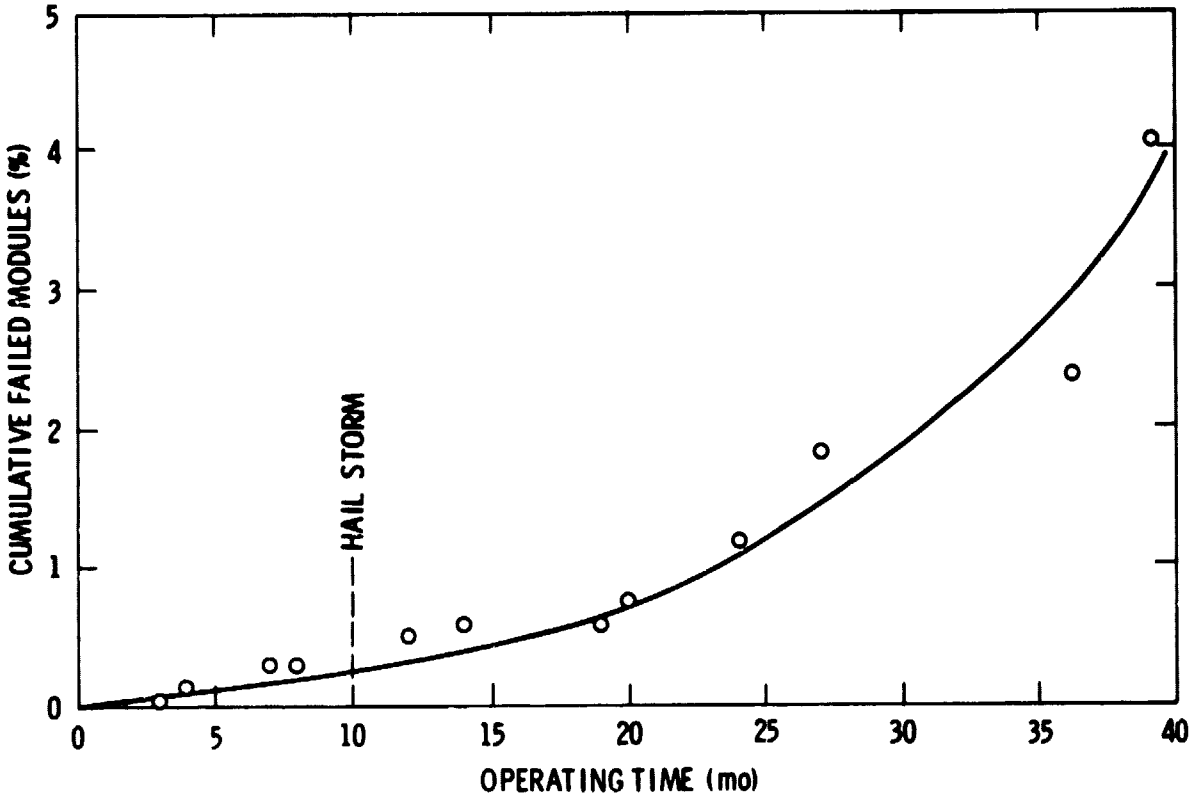

Figure 5-2. Solar Technology Block II Modules at the Mead Field-Test Site

Of the 2299 modules, 1024 were Sensor Technology modules (736 were Block II and 288 were Block III). Of these 1024 modules, 21 have failed because of either cracked cells or unsoldered interconnects.

Other studies by MIT-LL at their field-test sites centered on soil accumulation, the factor that had by far the greatest effect on overall power output. Power losses of Sensor Technology Block II modules range from 9.9% at Mead, to 43.3% at New York University.

Sensor Technology Block II modules have also been included at 16 field-test sites operated by JPL. These field-test sites are located from the Canal Zone, Panama, to Fort Greeley, Alaska, and have been active for up to 4 years. Almost all of the test sites have reported some type of degradation. A summary of these field observations is given in Table 5-3.

Table 5-3. Field-Test Site Observations of Sensor Technology Block II Modules

Discrepancy	No. of Sites Reporting Discrepancy (Of 16 Total)
Output terminal discoloration	10
Cell cracking (hail & other)	5
Split encapsulant	5
Edge seal delamination	4
Cell metallization discoloration	3
Bird damage	3
Interconnect breakthrough	3
Mesh discoloration	2
Encapsulant swelling	1
Interconnect corrosion	1

SECTION VI

JET PROPULSION LABORATORY TEST RESULTS

All ten of the Sensor Technology modules, which were used in the test-design evaluation, were inspected prior to aging and at least once every 30 cycles until the end of the test. Inspection included power output and electrical continuity measurements, as well as detail observation of physical changes of module materials.

A. OBSERVATIONS

Manufacturing defects, such as chipped cell edges, encapsulant inclusions (debris and bubbles), and split or scratched encapsulant were the main discrepancies that were initially observed. A few random areas of encapsulant repair (repotting) were also noted. None of these discrepancies, however, were seen to increase, spread, or act interactively during the length of the test.

All of the as-received modules exhibited significant encapsulant yellowing around the O-ring electrical seals. This was traced to a reaction between the room-temperature vulcanized (RTV) rubber encapsulant and the plasticizer in the O-ring seal. The discoloration did not change during the test and appeared to have no effect on the stability of module performance.

Clear RTV silicone rubber is well known to be a stable encapsulation system. This fact was confirmed by chemical analyses performed on the modules before and after the 360 cycles of accelerated aging. Infrared analysis of the pottant revealed a trace of ester, which was finally identified as an independent contaminant rather than a chemical reaction or breakdown by-product. There was a conspicuous lack of an -OH peak, indicating that no oxidation had occurred during the span of the test. EDAX analysis, using the scanning electron microscope, indicated that the SO_2 in the chamber atmosphere had reacted with neither the encapsulant nor the copper interconnects.

The only changes in module materials that could be linked to the encapsulant were delaminations. Figure 6-1 shows that, only delaminations at and around interconnects occurred at substantial rates. It can also be noted that Part No. (P/N) 20-10-1452, Revision J, had a higher incidence of these discrepancies than the same P/N for the Revision K modules. The Revision K modules incorporated a metal sheet over which the cells were encapsulated (see Figure 6-2). This somewhat isolated the cells from the thermal expansion of the silicone rubber in the backside stiffening ribs. Revision J did not have this metal sheet and, as a consequence, appeared to suffer from significantly more mechanical "working" of the interconnects during thermal cycling.

B. ELECTRICAL MEASUREMENTS

Electrical evaluation of the ten modules included LAPSS testing normalized to 28°C and continuity measurements at 95°C. Individual values

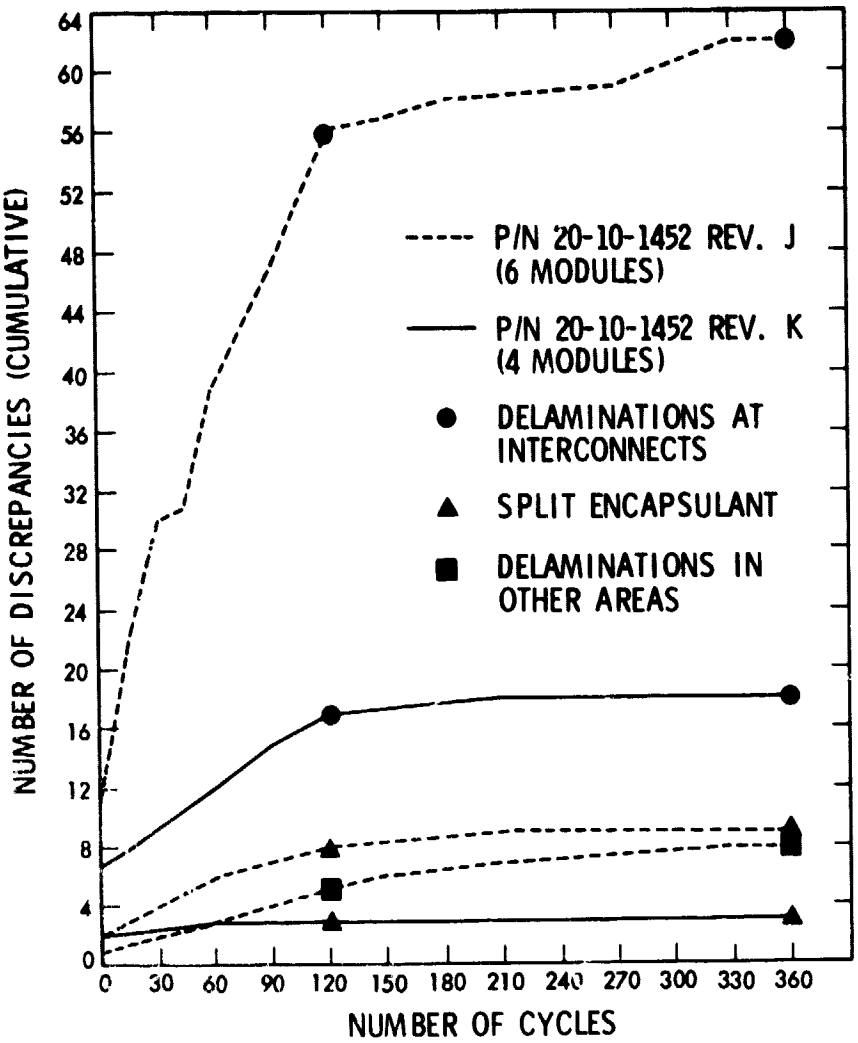

Figure 6-1. Observed Encapsulant Changes During Chamber Testing

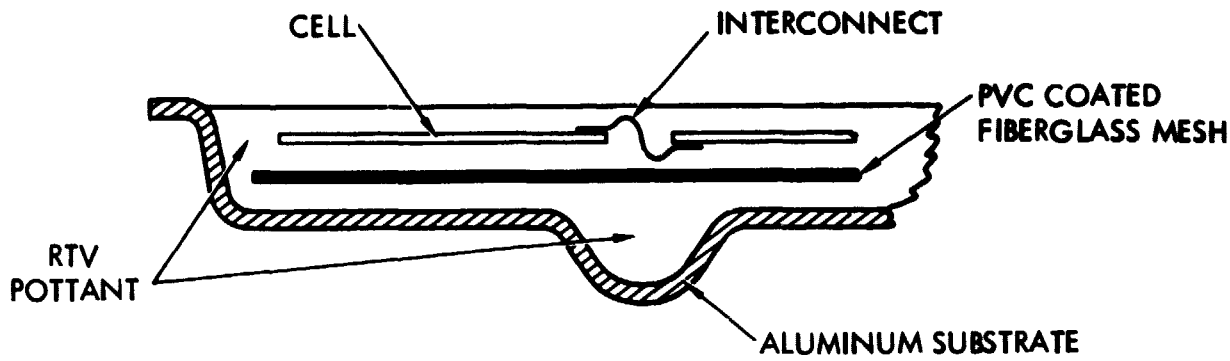

a. P/N 20-10-1452, Revision J

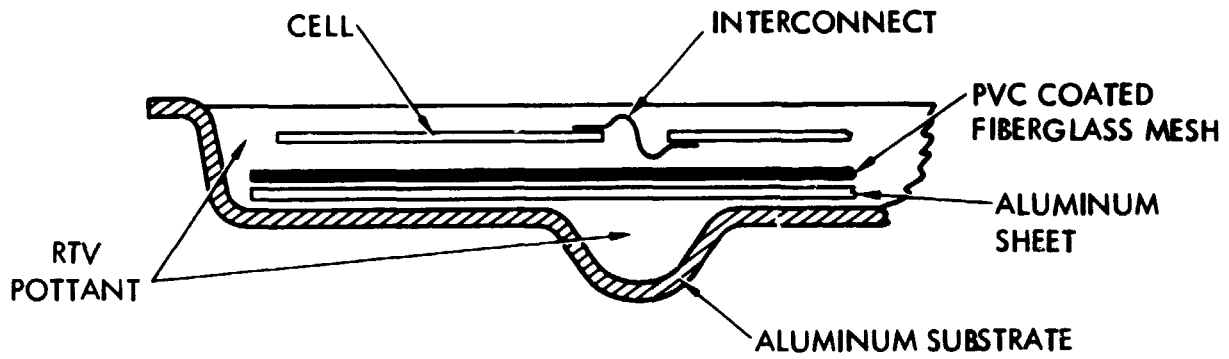

b. P/N 20-10-1452, Revision K

Figure 6-2. Module Designs and Materials

for $P_{(t)}$ were taken from the I/V curves that were generated by the LAPSS. Normalized power output as a function of time for each of the modules is shown in Figure 6-3. It should be noted that the values for one module [Serial No. (S/N) 3191] has been omitted as it suffered an impact cell crack during handling.

Between 150 and 210 cycles, it became evident that some significant mode of module degradation had surfaced. A plot of average normalized power output versus time (Figure 6-4) and the open circuit at room temperature of module S/N 3934 resulted in the conclusion that what was actually being observed was a direct result of an increase in electrical discontinuities caused by interconnect fatigue failure. This was substantiated both visually and by observation of a gradual decrease in electrical continuity at 95°C (Figure 6-5).

After 360 test cycles, electrical continuity was measured as a function of temperature. The data, shown in Figure 6-6, along with the measured Nominal Operating Cell Temperature (NOCT) of Sensor Technology Block II modules indicated that nearly 60% of the modules suffered complete (0 output)

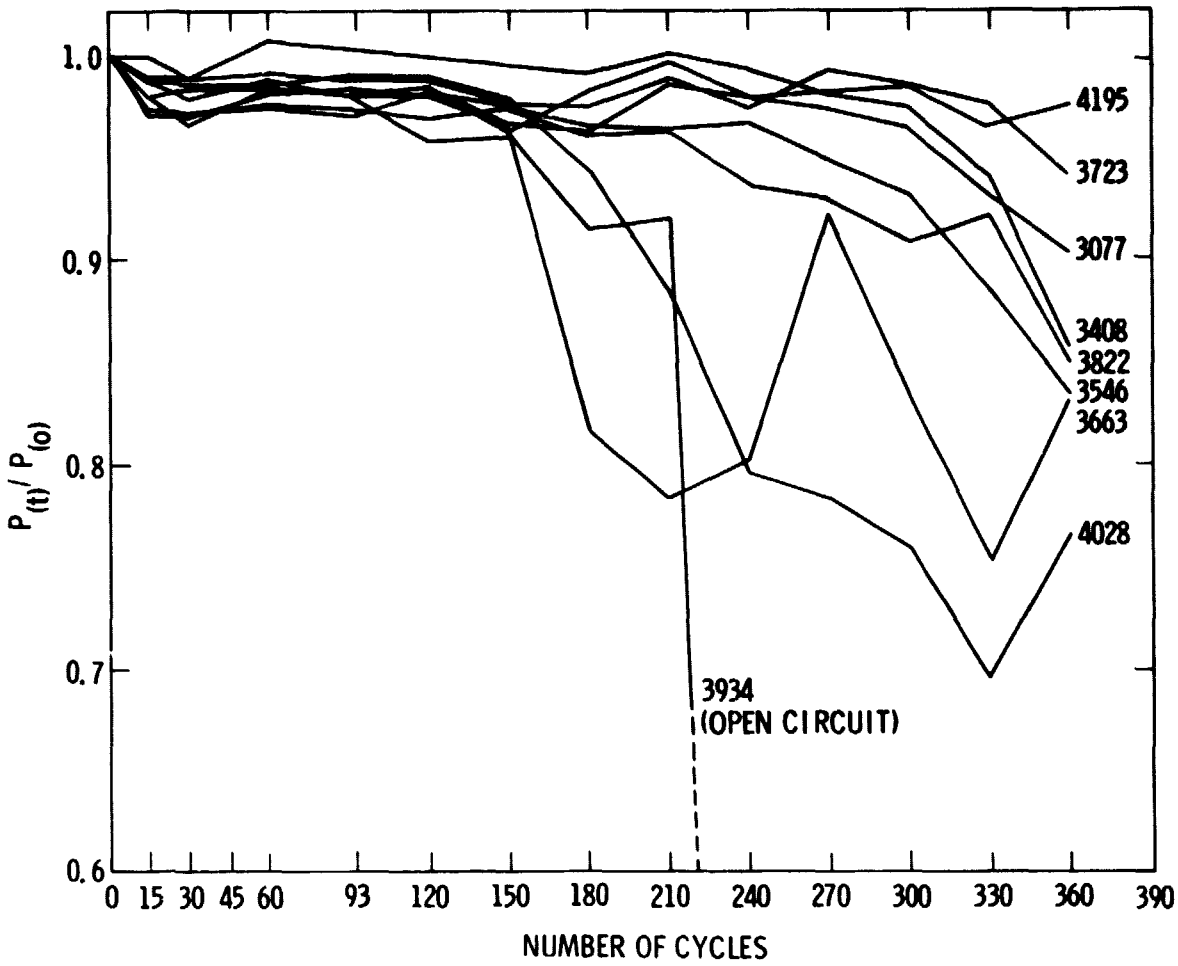

Figure 6-3. Power Output Loss (at 28°C) Caused by Chamber Aging Test

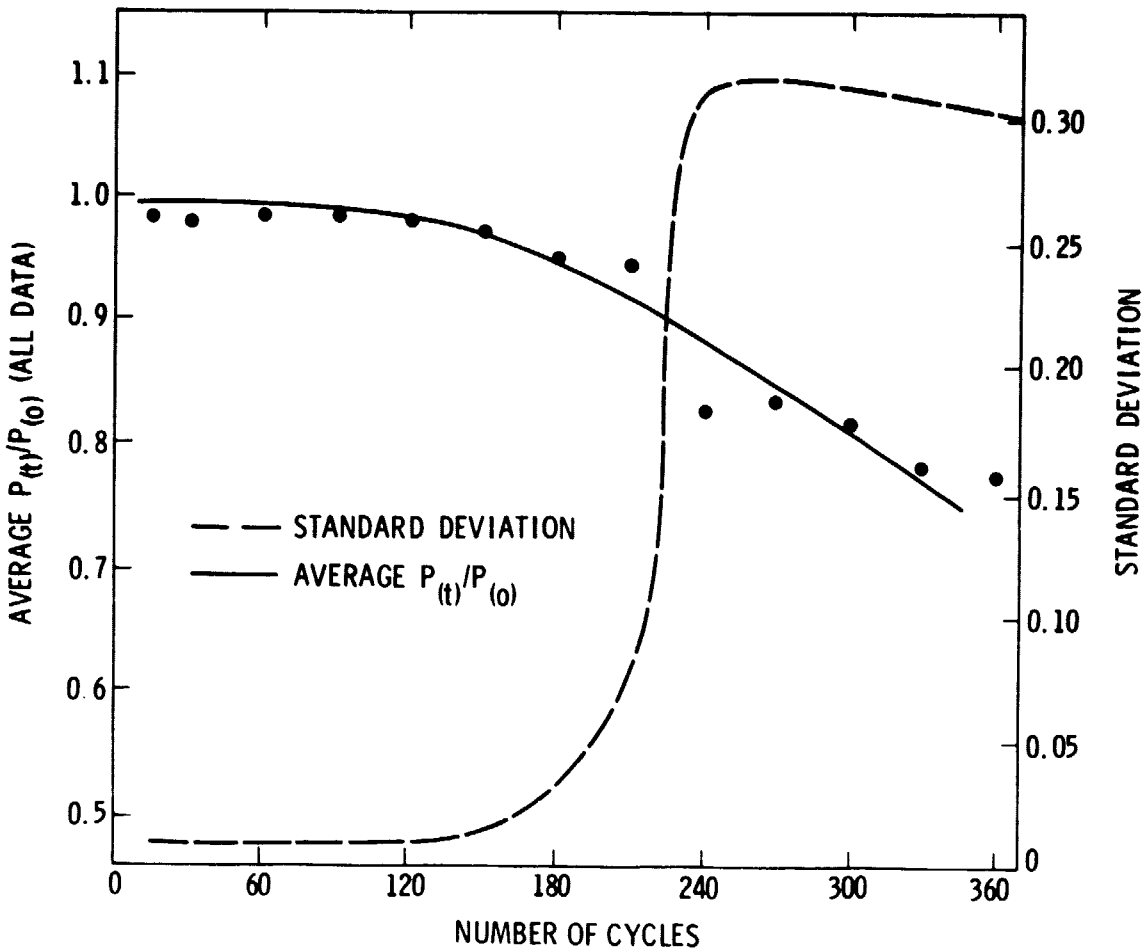

Figure 6-4. $P_{(t)}/P_{(o)}$ at 28°C versus Cycle Number (All Data) in LAPSS Tests

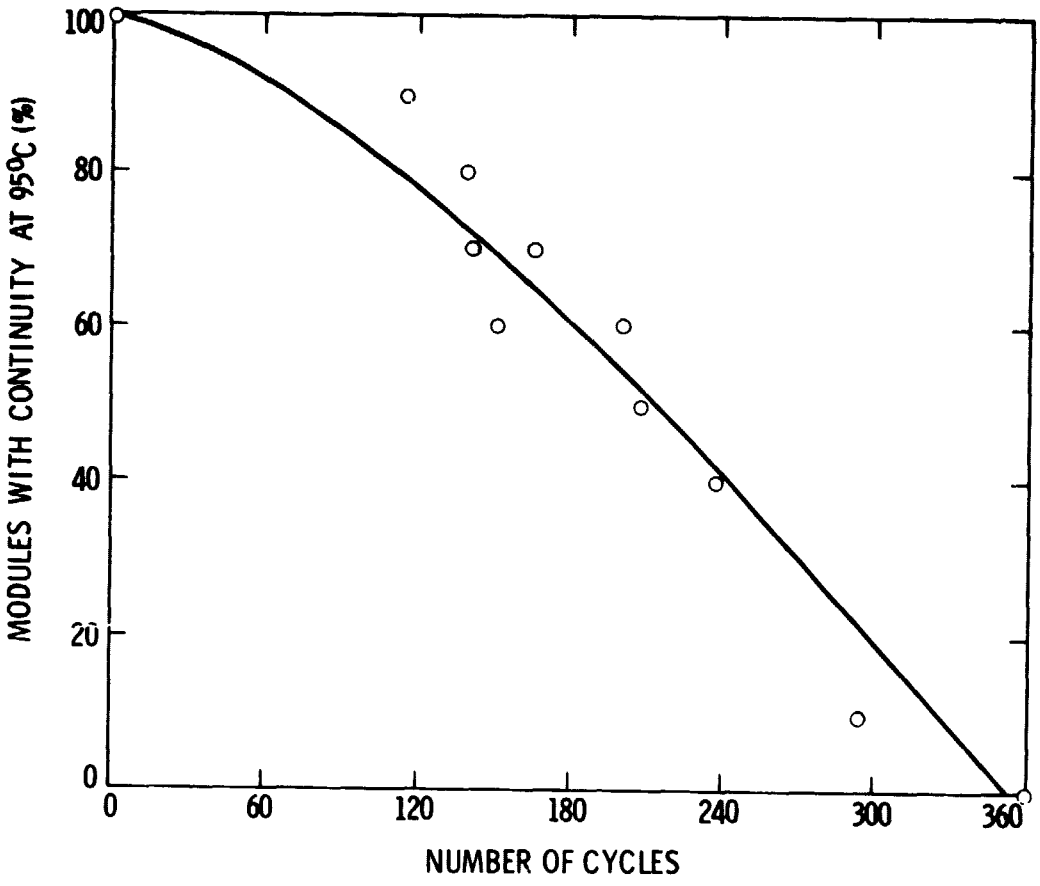

Figure 6-5. Electrical Continuity Loss During Testing

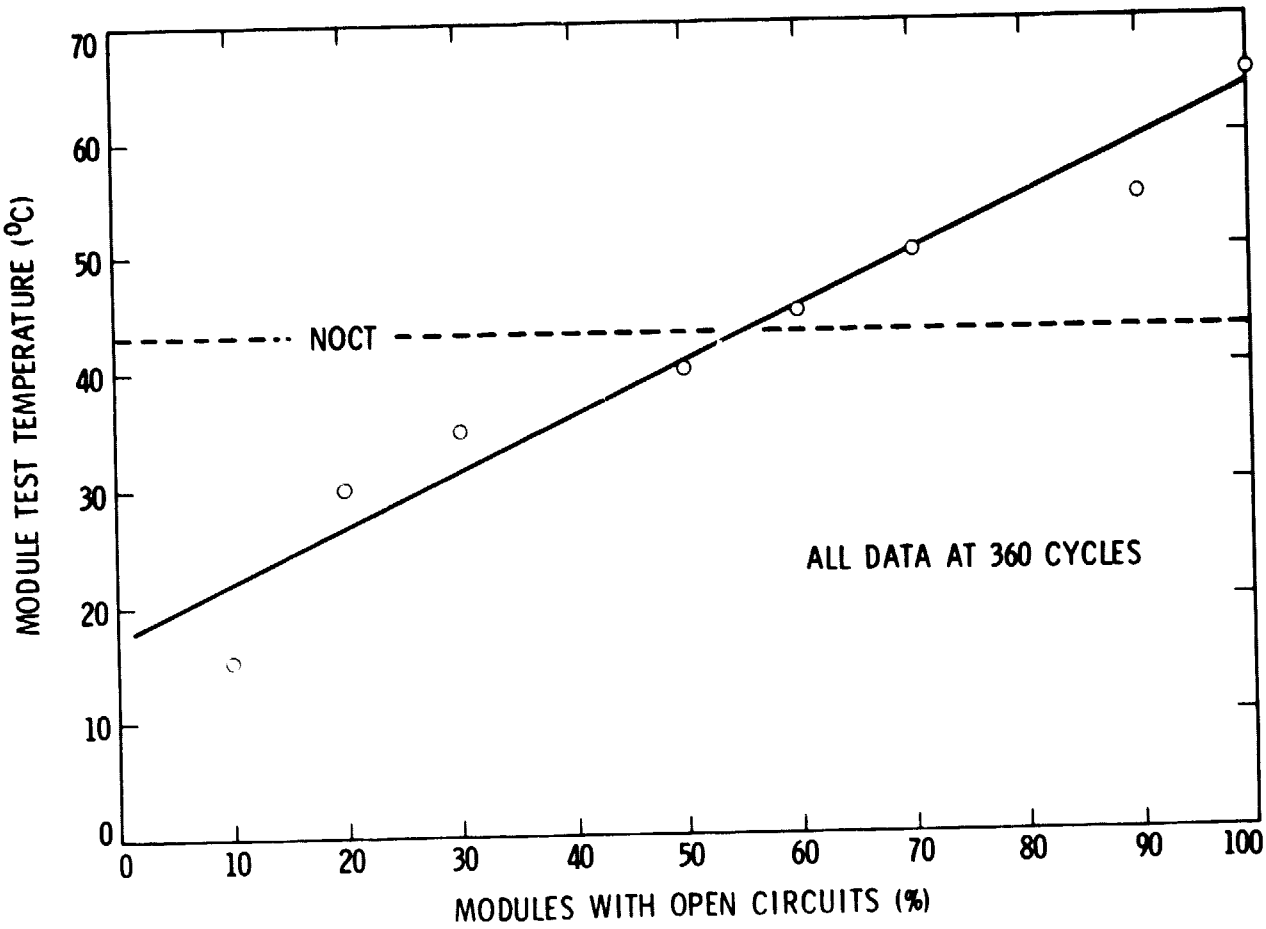

Figure 6-6. Module Continuity Loss versus Module Temperature

failure at NOCT. The test was terminated at this point because other fundamental chemical/physical modes of material degradation were apparently being masked by the effect of interconnect fatigue failure.

An attempt was made to provide some discrimination between the more subtle materials degradation effects and the somewhat erratic gross electrical failures. This was done by assuming that the module output values at a given time were samples of a normally distributed population. It was further assumed that this sample contained random intermittent discontinuities. The data was then evaluated by using Grubb's criteria for testing outlying observations (Reference 7). The resultant plot of $P_{(t)}/P_{(o)}$ versus time is shown in Figure 6-7. This curve probably more accurately reflects any of the fundamental materials changes that might have occurred. Unfortunately, the general assumptions required for the statistical analysis preclude reaching specific and meaningful conclusions from the data.

The effect of omitting the outlying data was evaluated by determining k and β for both sets of data. By rearranging Equation (1) and substituting Y for $P_{(t)}/P_{(o)}$,

$$1 - kt = Y^{\beta} \tag{4}$$

$$t = k^{-1}(1 - Y^{\beta}) \tag{5}$$

Allowing the function S to be defined as

$$S = \sum [t - k^{-1}(1 - Y^{\beta})]^2 \tag{6}$$

it can be seen that for a group of paired data points (t_i, Y_i) which satisfy Equation (1):

$$S = 0 \tag{7}$$

and

$$\frac{\partial S}{\partial k} = 0 = \sum [t - k^{-1}(1 - Y^{\beta})](1 - Y^{\beta})k^{-2} \tag{8}$$

$$= \frac{1}{k^2} \sum t(1 - Y^{\beta}) - \frac{1}{k^3} \sum (1 - Y^{\beta})^2 \tag{9}$$

By rearrangement, the constant K_1 may be defined as

$$K_1 = \frac{\sum (1 - Y^{\beta})^2}{\sum t\ (1 - Y^{\beta})} \tag{10}$$

By differentiating S with respect to β:

$$\frac{\partial S}{\partial \beta} = 0 = \sum [t - k^{-1}(1 - Y^{\beta})](\frac{1}{k})(Y^{\beta})\ \ln Y \tag{11}$$

$$= \frac{1}{k} \sum t(Y^{\beta})\ \ln Y - \frac{1}{k^2} \sum (1 - Y^{\beta})(Y^{\beta})\ \ln Y \tag{12}$$

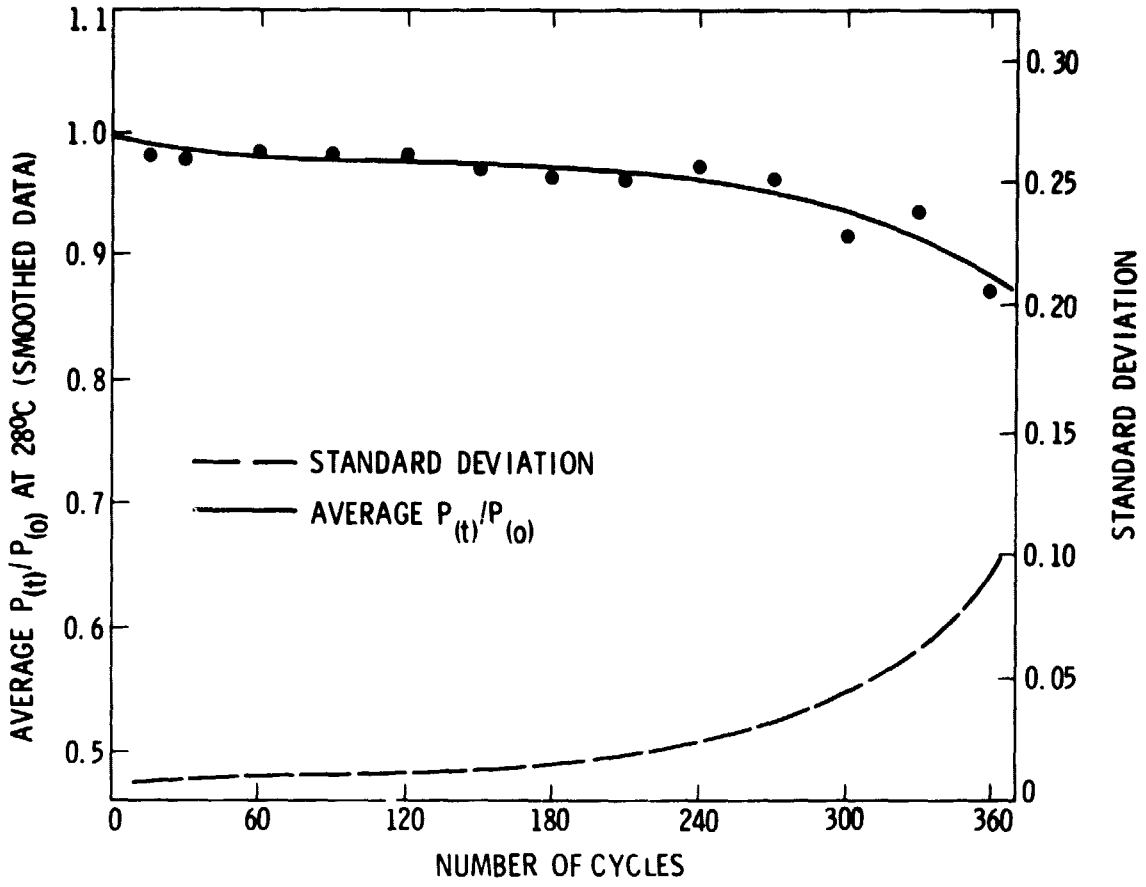

Figure 6-7. $P_{(t)}/P_{(0)}$ at 28°C versus Cycle Number (Smoothed Data) in LAPSS Tests

A second constant K_2 may now be defined:

$$K_2 = \frac{\sum (1 - Y^{\beta})\, Y^{\beta} \ln Y}{\sum tY^{\beta} \ln Y} \qquad (13)$$

There are now two equations (10 and 13) in terms of $K = f(\beta)$. These were then iterated on β until both equations converged on the same value, arriving at the best fit value for k and β. The results of the iterations for both sets of data are shown in Table 6-1. It should be noted that the least squares calculations incorporated all of the data points whereas the least squares average error omitted all data points above the computed 1/k cycles. The lower least squares average error for the smoothed data indicates that the statistical tests, which were used to eliminate outlying $P_{(t)}/P_{(0)}$ values, did result in a group of data that more closely obeyed the relationship shown in Equation (1).

The calculated values for k and β were substituted into Equation (1) and the resultant curves are presented along with those of the observed data in Figure 6-8. There is clear divergence between the model and the observed data after approximately 150 cycles.

Table 6-1. Least Squares Results For k and β

Population	k	β	Least Squares Average Error
All Data	0.0033	28.23	0.1576
Smoothed Data	0.0030	24.14	0.0438

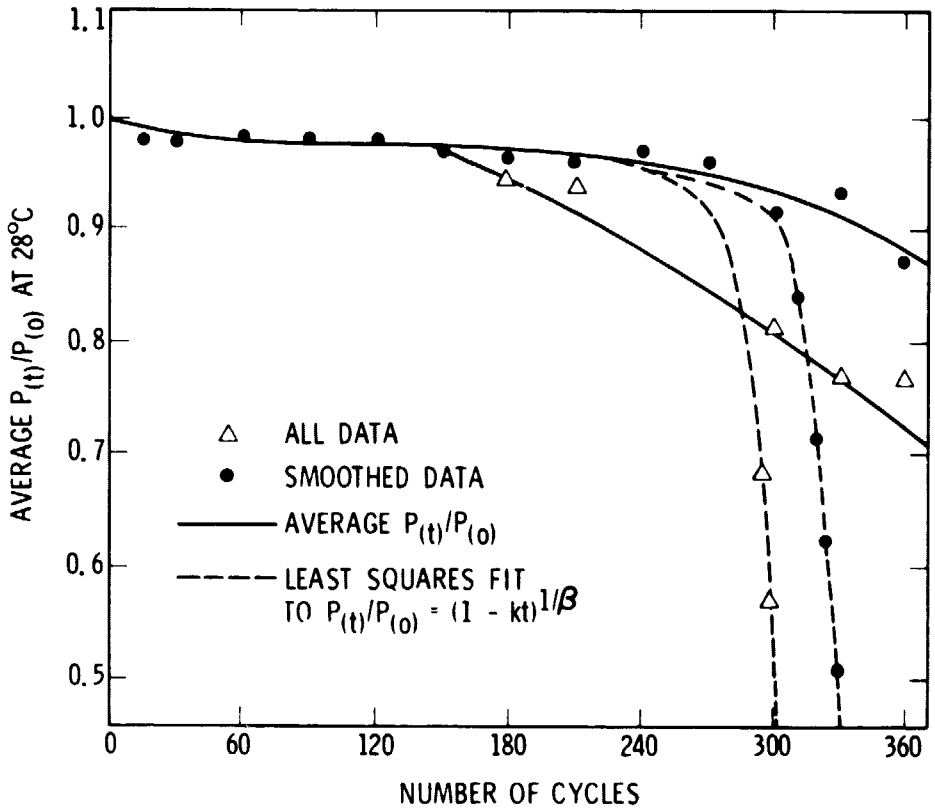

Figure 6-8. Observed and Modeled Module Performance

C. INTERCONNECT FATIGUE

As previously shown, the first module to exhibit an open circuit at 95°C did so in the 90 to 120-cycle regime. This was approximately the same time at which stress whitening of interconnects was first observed. Figure 6-9 illustrates the increasing frequency of this stress marking and subsequent

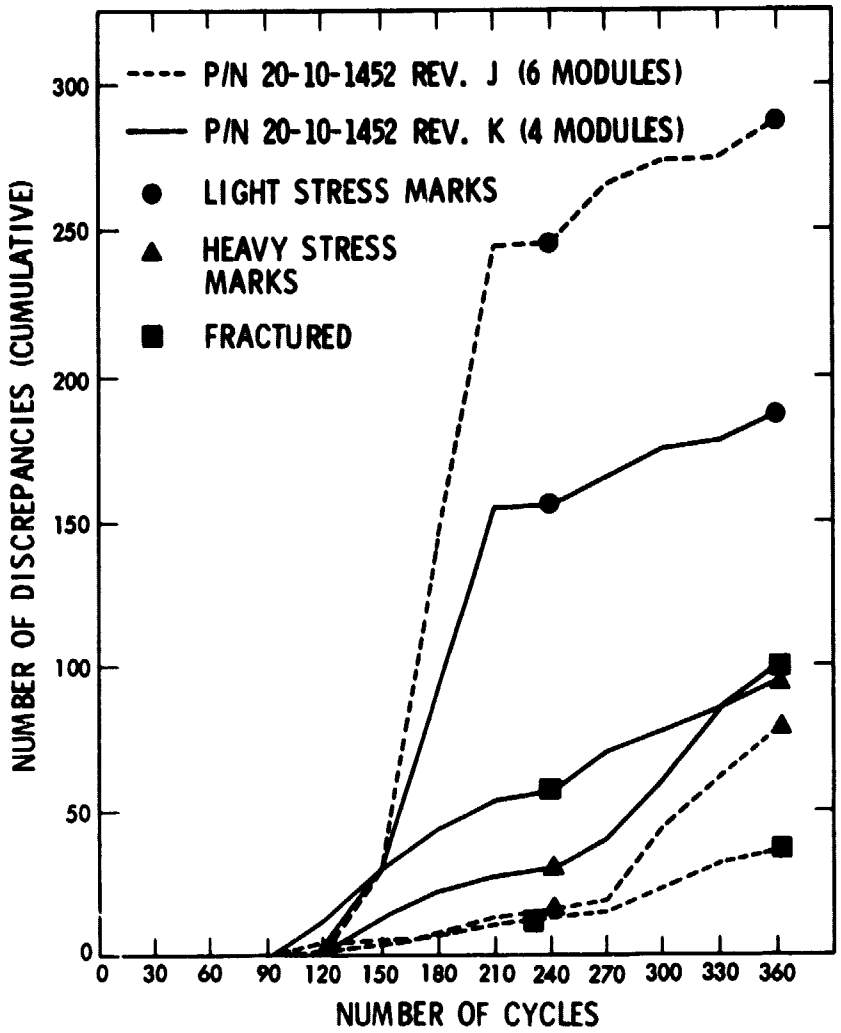

Figure 6-9. Observations of Interconnect Fatigue Phenomena in Ten Modules With 90 Interconnects per Module

fracturing of individual interconnects as a function of cycle number. There appeared to be little difference between the two designs of panels (P/N 20-10-1452, Revisions J and K) when the data was considered in light of their respective populations (six and four modules, respectively).

Figure 6-9 only describes the observed onset of the discrepancy. Hence, the plot of light stress marks continually increases even though many of the light stress-marked interconnects progressed through heavy marking and on to full fracturing.

Failure analysis was performed on module S/N 3934 after a complete open circuit was observed at 240 cycles. Electrical measurements revealed both interconnects of one cell to be completely fractured. These fractured interconnects, which were representative of others that were observed, are shown in Figures 6-10 through 6-13.

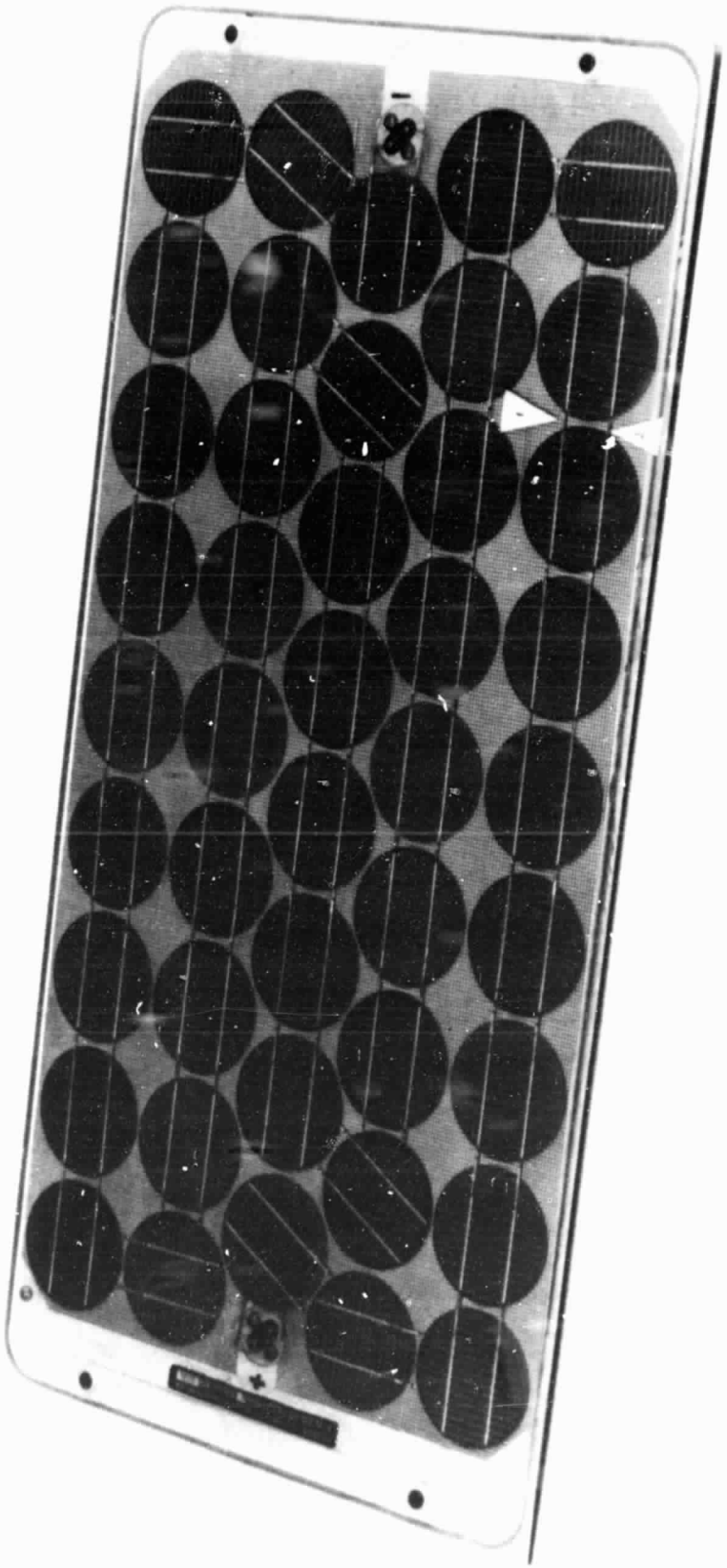

Figure 6-10. Sensor Technology Block II Module (S/N 3934)

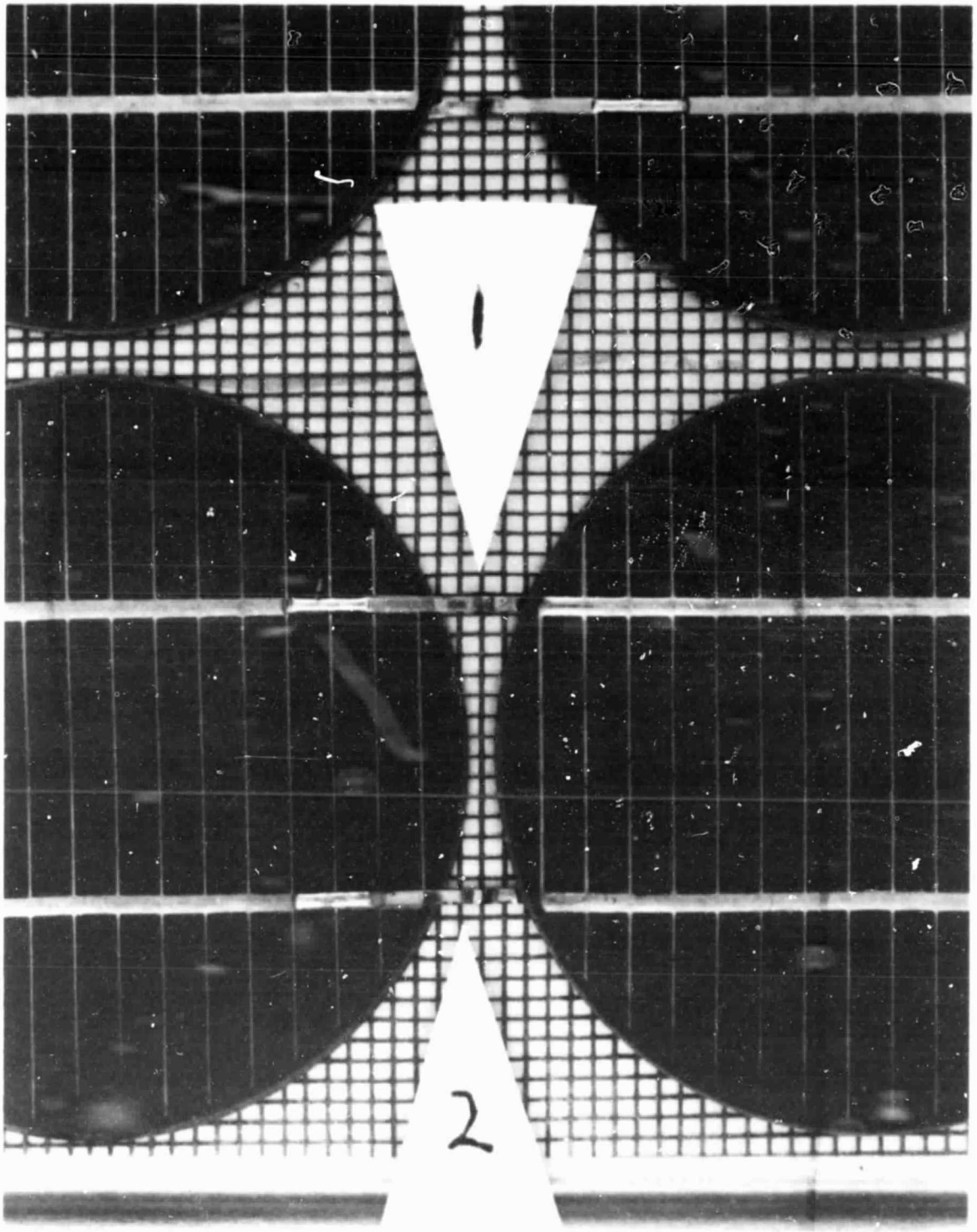

Figure 6-11. Fractured Interconnects

Figure 6-12. Interconnect Fracture No. 1

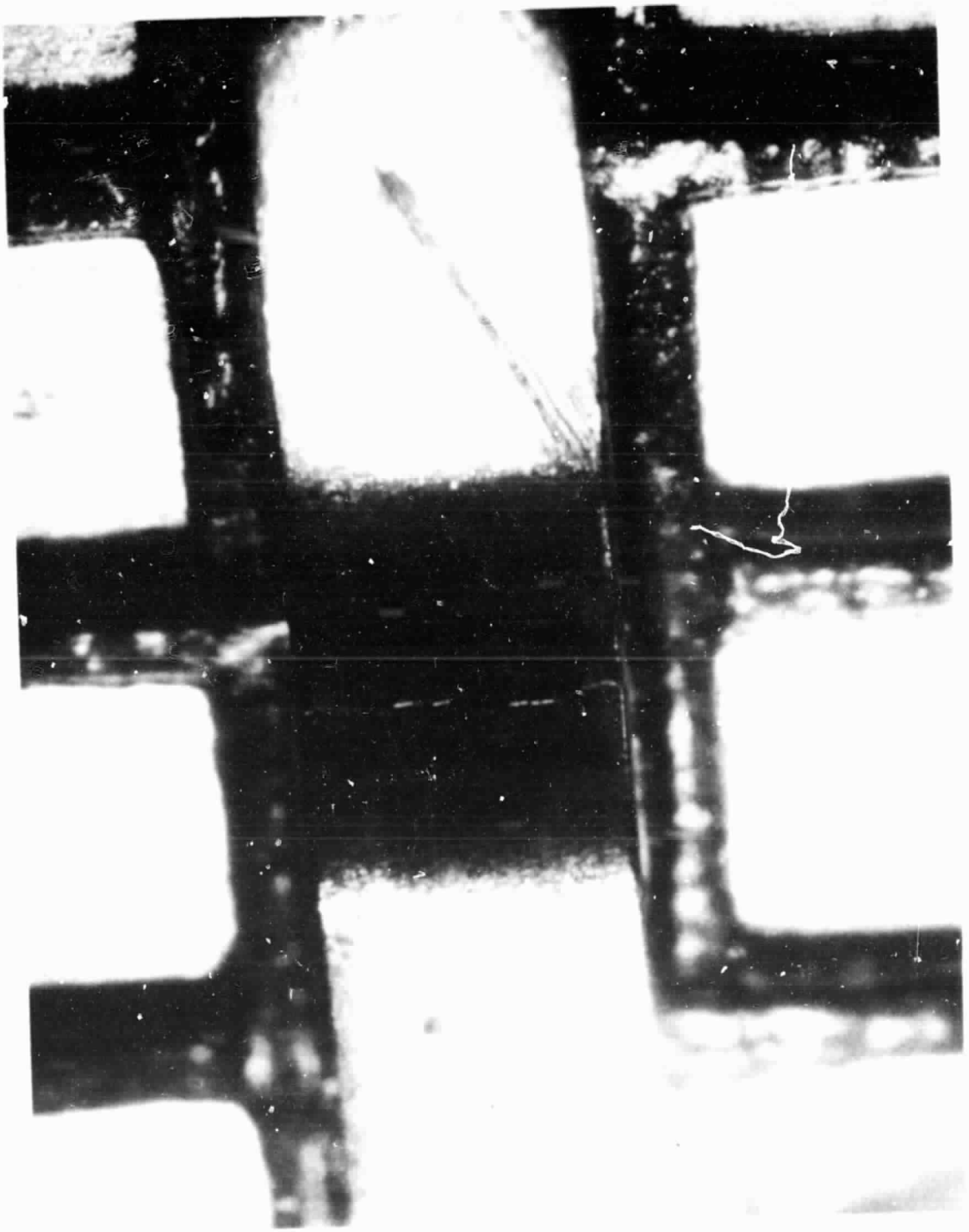

Figure 6-13. Interconnect Fracture No. 2

There has been considerable effort by G. Mon and D. Moore to characterize interconnect fatigue failure rates in terms of failure probabilities (Reference 8). Based on their work, the probability of interconnect fatigue resulting in module failure under field conditions may be estimated by using the observed failure rates that result from accelerated thermal cycling.

Because all of the cells in the Solar Technology Block II modules were connected in series with double interconnects, the probability of module failure (P_m) may be related to the probability of interconnect failure (P_I) by:

$$P_m = 1 - (1 - P_I^r)^n \tag{14}$$

where r is the interconnect redundancy, and n is the number of interconnect groups. For this design, r = 2 and n = 45.

With the observation that at NOCT approximately 55% of the modules were exhibiting open circuits after 360 cycles (see Figure 6-6), an observed failure probability is calculable:

$$P_m = 0.55 = 1 - (1 - P_I^2)^{45} \tag{15}$$

$$P_I = 0.133 \tag{16}$$

This failure probability was observed in a cyclic-temperature test that ranged from -15°C to +95°C, a span of 110°C. However, the average diurnal temperature variation at Mead, Nebraska, is approximately 33°C. A strain range conversion factor (ϵ_f) may be defined as:

$$\epsilon_f = \frac{T_{test}}{T_{field}} \tag{17}$$

$$= \frac{110}{33} = 3.33 \tag{18}$$

Using the set of fatigue curves developed by G. Mon and D. Moore (Figure 6-14), one may now estimate the field-time-to-failure for various failure probabilities as follows:

(1) At cycles = 360 read vertically to the curve approximating $P_I = 0.133$.

(2) Read laterally to find the test strain range $\Delta\epsilon_T \cong 0.013$.

(3) Convert to the field strain rate using ϵ_f: $\Delta\epsilon_T/\epsilon_f = 0.013/3.333 = 0.0039$.

(4) Read horizontally across from $\Delta\epsilon = 0.0039$ to the curve approximately $P_I = 0.133$.

(5) Read down to find the estimate of field cycles that can be expected to produce 50% module failures.

This procedure results in an estimate of approximately 9000 field days (24.7 years) to produce 50% module failures (P = 0) from interconnect fatigue. By similar analysis, it can be seen that 10% module failures may be expected after approximately 3300 field days (9 years). This series of curves and intercepts may thereby be used to estimate values of P_I for any number of test cycles or, similarly, they may be used to estimate the minimum number of test cycles a module must survive to guarantee a given P_I after 20 years in the field.

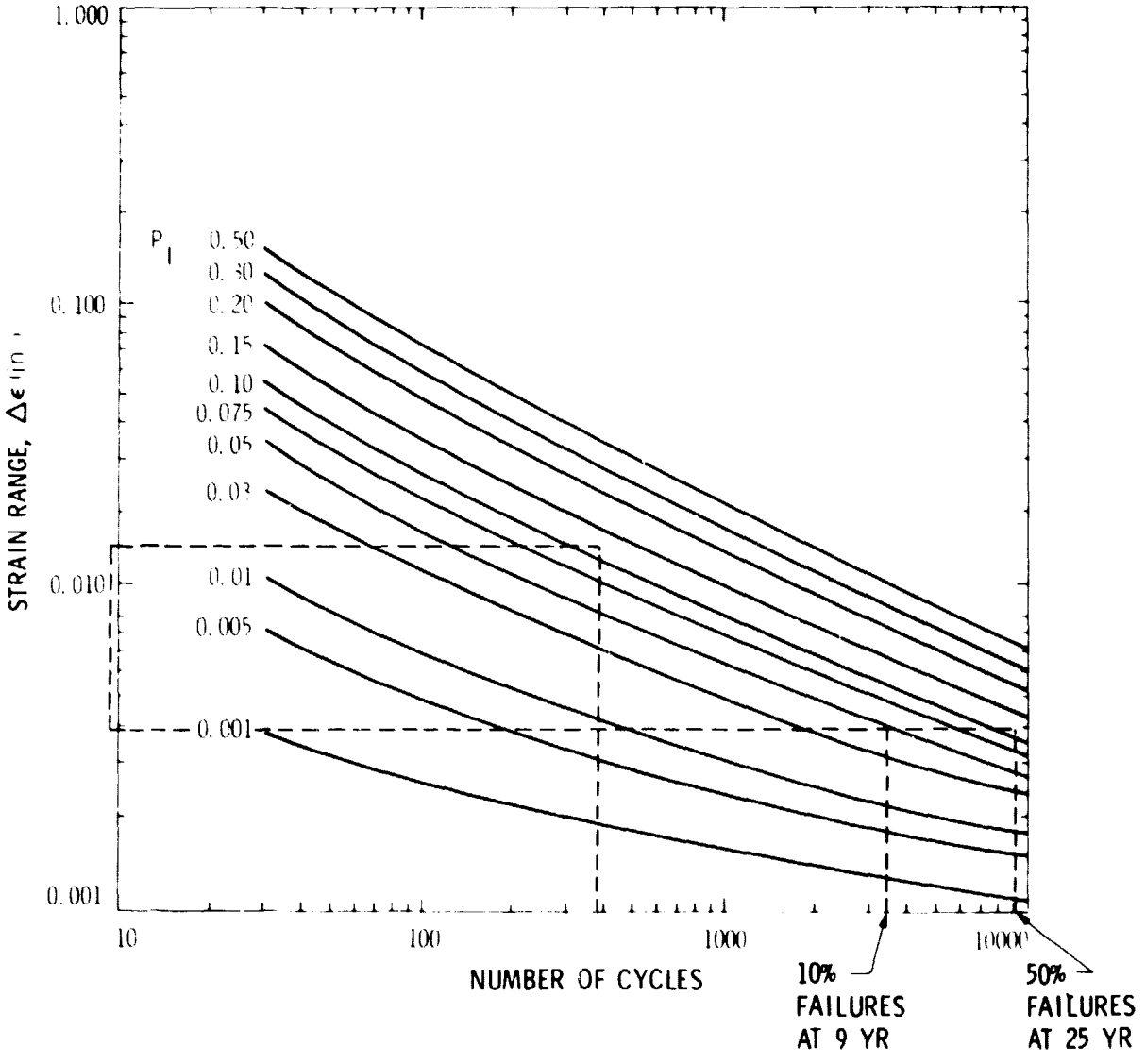

Figure 6-14. Interconnect Fatigue Failure Probabilities for Cyclic-Temperature Tests

SECTION VII

SUMMARY AND CONCLUSIONS

The purpose of this test design was to provide a method for evaluating the 20-year performance of solar modules with 2 years or less of accelerated testing. Such an accelerated test should increase the rates of individual and interactive modes of degradation, but should not change the fundamental mechanisms of degradation. Specifically, to have the confidence required to reach meaningful conclusions, the life-limiting mode of failure must be the same in the accelerated test as in the field application.

The test design was found to accelerate some of the modes of degradation, notably encapsulant delamination and interconnect fatigue. A summary of the expected and observed effects of chamber cycling is presented for comparison to field observations in Figure 7-1. Conspicuously missing from the observed effects is non-impact cell cracking. As previously discussed, this was a severe mode of degradation in the field, which has been linked to significant power losses at the Mead site and elsewhere. Why the test did not produce this effect is not clear at this time. It is also important to note that although at this time no failures in the field have been attributable to interconnect fatigue, this was the predominant cause of power loss during the test.

The accelerated tests introduced a new, life-limiting mode of failure and excluded a well-known mode of degradation, which indicate a fundamental limitation in the proposed test-chamber cycle. This is compounded by the poor agreement between the proposed performance model [Equation (1)] and the observed data during the test. As a result, it is not recommended that this form of accelerated test design be used to predict the 20-year performance of Sensor Technology Block II-type modules in the Mead, Nebraska, environment.

OBSERVED EFFECT	MEAD	CYCLED EXPECTED	CYCLED OBSERVED	JPL LOCAL	JPL REMOTE	MIT REMOTE
DISCOLORATION - RTV, YELLOW		(X)	X	X	X	
DISCOLORATION - MESH, WHITE				X	X	
SPLIT ENCAPSULANT	X		X	X	X	
CRACKED CELL (NON-IMPACT)	X	X		X	X	X
CRACKED CELL (IMPACT) [a]	X		(X)	X	X	X
EDGE SEAL DELAMINATION	X	(X)	X	X	X	
GRID DISCOLORATION				X	X	
INTERCONNECT BREAKTHROUGH [b]	X			X		
BIRD DAMAGE [a]				X	X	
INTERCONNECT DAMAGE		X			X	
INTERLAMINAR DELAMINATION	X	X	X	X		
ENCAPSULANT SWELLING				X		
INTERCONNECT FAILURE		X	X			
UNSOLDERED INTERCONNECTS [b]						X
SOILING	X			X	X	X
INCREASE IN SERIES RESISTANCE		X	X			

[a] RESULT OF A NON-INTERACTIVE STRESS

[b] RESULT OF MANUFACTURING DEFECT

Figure 7-1. Observed and Expected Test Results

REFERENCES

1. Gaines, G.B., et al., Methodology for Designing Accelerated Aging Tests for Predicting Life of Photovoltaic Arrays, ERDA/JPL-954328-77/1, Jet Propulsion Laboratory, Pasadena, California, February 1, 1977.

2. Noel, G.T., et al., Measurement Techniques and Instruments Suitable for Life-Prediction Testing of Photovoltaic Arrays, Interim Report, DOE/JPL-954328-78/1, Jet Propulsion Laboratory, Pasadena, California, January 15, 1978.

3. Noel, G.T., et al., Measurement Techniques and Instruments Suitable for Life-Prediction Testing of Photovoltaic Arrays, Final Report, DOE/JPL-954328-79/2, Jet Propulsion Laboratory, Pasadena, California, March 31, 1979.

4. Gaines, G.B., et al., Development of an Accelerated Test Design for Predicting the Service Life of the Solar Array at Mead, Nebraska, DOE/JPL-954328-79/13, Jet Propulsion Laboratory, Pasadena, California, June 7, 1979.

5. Griffith, J.S., Environmental Testing of Block II Solar Cell Modules, DOE/JPL-1012-79/1, Jet Propulsion Laboratory, Pasadena, California, January 1, 1979.

6. Forman, S.E., Performance of Terrestrial Photovoltaic Modules at MIT Lincoln Laboratory Experimental Photovoltaic Systems, DOE/ET-20279-140, Massachusetts Institute of Technology, April 30, 1981.

7. Grubbs, F.E., "Sample Criteria for Testing Outlying Observations," Doctorate Thesis, University of Michigan.

8. Mon, G.F., Moore, D.M., Ross, R.G. Jr., Interconnect Fatigue Design for Terrestrial Photovoltaic Modules, DOE/JPL-1012-62, Jet Propulsion Laboratory, Pasadena, California, March 1, 1982.

APPENDIX

$P_{(t)}/P_{(o)}$ DATA

No. of Cycles	Serial Number (S/N)								
	3077	3408	3546	3663	3723	3822	3934	4028	4195
0	11.36	11.09	10.19	10.48	10.74	10.54	11.57	11.31	10.96
15	0.974	1.000	0.974	0.972	0.990	0.988	0.980	0.989	0.980
30	0.973	0.989	0.973	0.971	0.989	0.979	0.966	0.987	0.984
45	-	-	-	-	-	-	-	-	-
60	0.976	1.009	0.978	0.981	0.993	0.989	0.984	0.985	0.983
93	0.972	1.005	0.975	0.984	0.989	0.980	0.982	0.990	0.982
120	0.983	1.000	0.969	0.981	0.988	0.980	0.958	0.990	0.984
150	0.968	0.995	0.975	0.969	0.978	0.975	0.960	0.969	0.964
180	0.964	0.992	0.967	0.815[a]	0.975	0.981	0.915	0.945	0.984
210	0.987	1.001	0.966	0.784[a]	0.989	0.965	0.920	0.887	0.996
240	0.979	0.993	0.969	0.802[a]	0.975	0.937	0[a]	0.795[a]	0.980
270	0.974	0.981	0.949	0.922	0.993	0.929	0[a]	0.783[a]	0.982
300	0.966	0.973	0.932	0.834	0.987	0.907	0[a]	0.759[a]	0.984
330	0.931	0.941	0.886	0.753[a]	0.977	0.922	0[a]	0.695[a]	0.967
360	0.906	0.857	0.834	0.831	0.941	0.855	0[a]	0.767	0.974

[a]Values rejected using Grubb's criterion.

Notes: (1) Values for 0 cycles are maximum power (Watts)

(2) 1 day = 3 cycles.

(3) 45-cycle data invalid.

(4) S/N 3191 data invalid and therefore not listed.